molecular pharmaceutics

pubs.acs.org/molecularpharmaceutics

Article

Peptide Spiders: Peptide–Polymer Conjugates to Traffic Nucleic Acids

Ester J. Kwon,*,○ Henry Ko,○ and Sangeeta N. Bhatia*

Cite This: *Mol. Pharmaceutics* 2020, 17, 3633–3642

Read Online

ABSTRACT: Therapeutic nucleic acids hold great promise for the treatment of genetic diseases, yet the delivery of this highly charged macromolecular drug remains a challenge in the field. Peptides are promising agents to mediate nucleic acid delivery because they can encode a biological function to overcome the trafficking barriers. Electrostatic nanocomplexes of nucleic acid and peptides can achieve effective delivery, but the balance between their stability and biological function must be finely tuned. In this work, we explore two peptide building blocks that have been studied in the literature: targeting ligands and intracellular trafficking peptides. We grafted these peptides on a polyethylene glycol (PEG) backbone with eight sites for substitution to create so-called "peptide spiders". These conjugates achieve stability via the well-known hydrophilic shielding effect of PEG. In addition, the coordination of peptide building blocks into multimers may create new biological properties, such as the well-known phenomena of increased binding avidity with multivalent ligands. In this work, we linked two trafficking peptides to the PEG backbone using either nonreducible or reducible chemistries and investigated the ability of these materials to carry silencing RNAs into mammalian cells. We then investigated these nanomaterials for their pharmacokinetic properties and silencing of undruggable targets in a mouse model of cancer. While reducible linkages were more potent at silencing in vitro, this effect was reversed when applied in the context of living animals. This work offers an insight into peptide-based delivery materials and investigates peptide–polymer linkages.

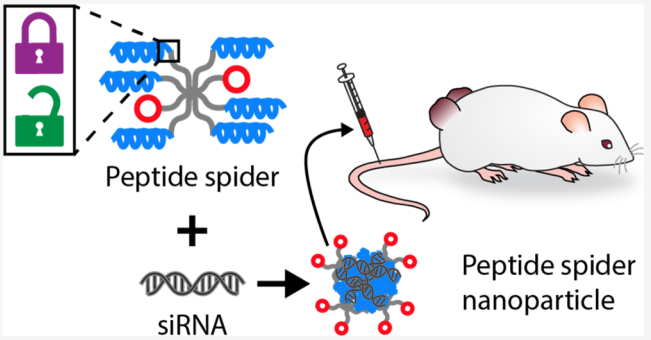

KEYWORDS: *peptides, polyethylene glycol, gene delivery, cancer*

1. INTRODUCTION

The delivery of nucleic acids to specific cell types within the body offers a promising therapeutic avenue to regulate gene expression for the treatment of disease. Potential cargoes include nucleic acids to induce gene silencing (siRNA, miRNA), gene expression (mRNA transcripts, plasmid DNA), and CRISPR-based gene editing. To achieve nucleic acid delivery, the challenge is to chaperone a highly charged macromolecule so that it can navigate several biological hurdles including maintaining stability in the blood, extravasation into tissue, uptake in cells of interest, and intracellular trafficking to specific subcellular compartments. Nanoparticles (NPs) offer a solution to address the challenges of nucleic acid delivery because they can be programmed with multiple functions into a single entity, such as protection and condensation of macromolecular cargo and trafficking through multiscale biological barriers.[1,2] In addition, NPs can assemble hundreds of molecules in an organized structure to create many advantages for drug delivery, for example, hydrophobic pockets for drug loading, co-delivery of drug combinations, and creating high local concentrations for improvement of therapeutic indices. Inspired by viruses, a natural NP, engineers have incorporated biological function using biomolecules to achieve trafficking.[3] Beyond biological function, the pharmacokinetics of the NPs must also be engineered and modern NP formulations incorporate molecules for stabilization; for example, ONPATTRO is the first synthetic siRNA NP drug approved by the FDA and includes polyethylene glycol (PEG) in its formulation.[4]

One class of biomolecules is peptides, which are attractive candidates for clinical translation because they can display selective biological function while maintaining biocompatibility.[5] Their development as therapeutics has been facilitated by technology to improve their stability, including chemical modifications[6] or assembly on nanostructures.[7] Peptides have been used to transfer nucleic acid cargos into cells, in particular peptides that interact with membranes to overcome entrap-

Received: July 6, 2020
Revised: July 8, 2020
Accepted: July 9, 2020
Published: July 27, 2020

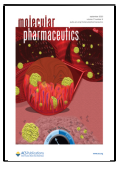

https://dx.doi.org/10.1021/acs.molpharmaceut.0c00714
Mol. Pharmaceutics 2020, 17, 3633–3642

ment in endocytic vesicles.[8−10] Another class of peptides that has been studied widely across the NP field includes peptides that act as ligands to mediate active targeting.[11−13] In previous work, we described a peptide-based approach for siRNA delivery that combines both of these functional elements and includes a domain for (1) tumor-targeting/penetration and (2) endosomal escape that electrostatically assemble with nucleic acid cargo.[14,15] The result was a two component system comprised of nucleic acid with trafficking peptide. Further refinements were made to this system to achieve stable vascular delivery, namely by exploring several architectures for the incorporation of PEG that preserved silencing activity.[16] This three component system was comprised of electrostatic complexation of nucleic acid with a trafficking peptide and peptide−PEG hybrid material. Both peptides and PEG have been widely investigated as components of nucleic acid delivery carriers,[17−19] and establishing strategies to engineer the structures of these materials has been an active area of research.[20−22] A remaining challenge is how to balance the seemingly conflicting goals of achieving stability in physiological solutions with the efficient cellular accumulation and release of cargo for successful delivery that presents a problem for many nonviral gene carriers when applied in vivo.[23−25] It is also the case that the incorporation strategy of PEG is dependent on the composition of the NP, and can include lipids, polymers, and metals.[26,27] Strategies to incorporate PEG into NPs composed predominantly of peptides without compromising activity has yet to be resolved.[28,29]

In this work, we designed a nucleic acid carrier material that allows for stoichiometric control of two biological units: tumor-targeting and intracellular trafficking. In order to target tumors, we used iRGD, a peptide discovered via in vivo phage display that binds to upregulated $\alpha_v\beta_3$ integrins on tumor cells and stroma.[30] We and others have shown that iRGD modification can increase the accumulation of multiple NP types (e.g., liposomes, polymeric NPs) into several tumor models.[14,30−33] We used transportan for intracellular trafficking, a membrane-active peptide that was identified in a screen of known cell penetrating peptides to increase intracellular delivery of siRNA cargo.[15] These biological units represented by peptides are coordinated on a multiarm PEG scaffold to promote stability of resulting NPs after electrostatic complexation of nucleic acids. In addition, presentation of multimers of each biological unit has the potential to enhance biological function that is represented in nature. For example, multivalent targeting ligands are known to improve avidity[34,35] and mediate differential biological responses.[36] In another example, viral proteins that insert in membranes for transfer of genetic material or membrane rupture often have repeating subunits[37] or can work as multiprotein structures.[38,39] Synthetic peptides derived from these proteins have membrane-associating properties, and their arrangement in multimers can increase their activity.[40] To take advantage of these multimer effects, we arrange both targeting−targeting ligands and intracellular trafficking peptides as multimers in this work. Previous work has explored multivalent peptides on polymer backbones,[41,42] although these studies were restricted to investigations in vitro; in the present work, we investigate the function of these materials in vivo. The challenge of predicting in vivo efficacy of nonviral gene carriers based on in vitro optimizations has been well-documented.[27,43] We investigated the role of attaching peptides with reducible or nonreducible bonds; although materials made with reducible disulfide bonds performed on par with those made with nonreducible bonds in in vitro silencing assays, materials with nonreducible bonds had improved performance when applied to animals bearing tumors. Overall, our work presents insights into the design principles of peptide-based electrostatic nucleic acid delivery NP, including a potential design for hydrophilic PEG stabilization and bond stability for the incorporation of trafficking peptides.

2. MATERIALS AND METHODS

2.1. Reagents. Peptides were synthesized by CPC Scientific to 90% purity. Transportan was synthesized with an N-terminal myristic acid and a C-terminal cysteine (myristic acid-GWTLNSAGYLLGKINLKALAALAKKILC) and iRGD was synthesized with an N-terminal azide (azidoacetyl-GGGCRGDKGPDC). The following siRNA sequences were synthesized from Dharmacon: siLuc (CUUACGCUGAGUACUUCGA), siID4 (equimolar mixture of GCGAUAUGAACGACUGCUUAU and CCGACUUUAGAAGCCUACUUU). All fluorophore modified siRNA was prepared by modifying the 5′ end on the sense strand. VivoTag-S-750 fluorophore was used for whole organ scans and siRNA encapsulation because this fluorophore is compatible with the LI-COR Odyssey imaging systems, DyLight 647 fluorophore was used for epifluorescence microscopy, and FAM fluorophore was used for immunohistochemistry because its signal can be amplified with antibody labeling.

2.2. Peptide Spider Conjugation. Eight-arm PEG (20,000 g/mol molecular weight) was purchased functionalized with OPSS (Creative PEGWorks) or maleimide (JenKem). The sizes of each PEG was verified by matrix assisted laser desorption/ionization (MALDI) and found to be 14,000 and 20 g/mol, respectively. To prepare peptide conjugates, 8.1 equiv. of peptide at the indicated stoichiometry was added to PEG in dimethylformamide and 50 mM trimethylamine. After reaction for 4 h in the dark, reaction was quenched with 100 mM cysteine for 15 min and dialyzed extensively into water using a 10,000 MWCO membrane for 4 complete exchanges.

2.3. NP Formulation and Characterization. Conjugate concentrations were calculated based on the absorbance of the tryptophan residue in transportan at 280 nm and 6 transportan peptides per conjugate. For all in vitro studies, NPs were formulated by adding equal volumes of conjugate to 2 μM siRNA in water at the indicated molar ratios and mixing rapidly. NPs were imaged with transmission electron microscopy (TEM) by adsorbing particles to grids and negative stained with tungstophosphoric acid. Particles were imaged with a JEOL 2100 FEG TEM. Hydrodynamic diameters were measured using an 850 nm laser with a Wyatt DynaPro Plate Reader between 30 min at 6 h after formulation of NPs. Zeta potential measurements were made on a Malvern Zetasizer Nano. NP concentration was measured with a Malvern NanoSight. For in vivo formulations, concentrations of conjugates and siRNA were ten-fold higher to create volumes suitable for in vivo administration.

2.4. Encapsulation Efficiency. NPs were formulated with VivoTag-S750-labeled siRNA at the indicated formulation ratios in triplicate. 6.7 pmol of siRNA was loaded per lane of a 2% agarose gel and imaged on a LI-COR Odyssey. Amount of siRNA was quantified for each formulation normalized to a free siRNA control using ImageJ software to determine encapsulation efficiency.

https://dx.doi.org/10.1021/acs.molpharmaceut.0c00714
Mol. Pharmaceutics 2020, 17, 3633−3642

2.5. Cell Culture. OVCAR-8 expressing firefly luciferase (OVCAR-8 Luc+) were a gift from Joyce Liu (Dana Farber Cancer Institute). U937 and MDA-MB-435S cells were obtained from ATCC. OVCAR-8 and U937 cells were cultured in RPMI 1640 media supplemented with 10% fetal bovine serum (FBS) and 1% penicillin & streptomycin (PS). MDA-MB-435S cells were cultured in Dulbecco's modified Eagle's medium supplemented with FBS and PS.

2.6. Silencing Activity and Toxicity. OVCAR-8 cells stably expressing luciferase were plated at 8000 cells/well in a 96-well tissue culture plate 24 h before transfection. NPs were formulated as described above with siLuc siRNA and added to cells in OptiMEM at less than 10% of the final volume. Cells were also transfected with Lipofectamine RNAiMAX (Invitrogen) according to manufacturer's instructions. Cells were incubated for 4 h and medium was replaced with culture media for an additional 48 h. Cell viability was measured by 3-(4,5-dimethylthiazol-2-yl)-5-(3-carboxymethoxyphenyl)-2-(4-sulfophenyl)-2*H*-tetrazolium (MTS) using the CellTiter AQueous One Cell Proliferation assay (Promega) according to manufacturer's instructions. Luciferase activity was measured by lysing cells with passive lysis buffer (Promega) and assaying 20 μL of lysate with 30 μL of luciferin (Promega). Luminescence was integrated for 1 s on a Tecan Infinite M200 Pro plate reader and normalized by the protein content measured by a bicinchoninic acid (BCA) assay (Pierce).

2.7. Intracellular Distribution. OVCAR-8 cells were grown for 24 h at ~50% confluency on coverglasses coated with 10 μg/mL poly-D-lysine. Cells were transfected as above at a final concentration of 100 nM Dy647-labeled siRNA formulated at a 4:1 ratio of peptide spider/siRNA and incubated at 37 °C for 2 h. Cells were then rinsed with phosphate-buffered saline (PBS) twice and fixed in 4% paraformaldehyde. Cells were stained for lysosome-associated membrane protein-1 (LAMP1; Abcam) and counterstained with phalloidin and Hoechst (Invitrogen) and imaged on a Nikon Eclipse Ti microscope.

2.8. Cell Association. Relative receptor expression was determined. U937 and MDA-MB-435S cells were harvested using enzyme-free cell dissociation buffer (Gibco) and incubated on ice for 15 min. Cells were blocked with 2% BSA, 10% donkey serum in PBS and cells were incubated with primary antibody against α_v integrin, $\alpha_v\beta_3$ integrin, or IgG control (BioLegend) for 1 h. To measure NP association, cells were harvested as above and 100,000 cells per condition were incubated with NPs formulated at a 4:1 ratio of peptide spider/siRNA with Dy547-labled siRNA at the indicated concentration for 2 h on ice. After washing with PBS, cells were analyzed on a BD LSR Fortessa HTS and analyzed with FlowJo software.

2.9. Pharmacokinetics of NPs in Animals. A flank xenograft mouse model was created by bilaterally implanting 5 to 10 × 10^6 MDA-MB-435 cells subcutaneously in 4−5 week old female NCR-nude mice (Taconic). Experiments were initiated when tumors had an average tumor volume between 200 and 300 mm^3 per flank. Mice were distributed to groups based on tumor size. To measure half-lives, NPs formulated with 1 nmol of VivoTag-S 750-labeled siRNA at 4:1 ratio of peptide spider/siRNA in 5% dextrose were injected intravenously and 10 μL of blood was drawn at 0, 5, 15, 30, 60, and 120 min post injection. Biodistribution of NPs in organs was determined by harvesting organs at 3 h post injection and homogenizing samples in a hypotonic 1% SDS, 18 mM Tris, pH 7.4 buffer. Samples were then boiled and cleared before measuring fluorescence of VivoTag-S 750 in the tissue supernatant.

2.10. Imaging of NPs in Tumors. Tumors were implanted in mice as above and treated with NPs prepared with 1 nmol of FAM-labeled siRNA at 4:1 ratio of peptide spider/siRNA injected at 24, 3, and 1 h(s) prior to harvesting of tumors. Tumors were fixed with 4% paraformaldehyde and 10 μm frozen sections were prepared. FAM signal was amplified with the VectaFluor R.T.U. kit (Vector Laboratories) as per manufacturer's protocol. Sections were imaged on a Pannoramic 250 (3DHISTECH).

2.11. In Vivo Silencing Activity. NPs were formulated at 4:1 ratio of peptide spider/siRNA using 2 nmol of a 1:1 mixture of two ID4 siRNA sequences. NPs were injected intravenously in a 5% dextrose solution 6, 4, and 2 days before harvesting tumors. Tumors were frozen on dry ice and homogenized in lysis buffer supplemented with protease inhibitors. Western blot analysis was performed on lysates with antibody against ID4 (Abcam) and normalized by tubulin (Invitrogen). Quantification of protein was done by calculating area under the curve using ImageJ software.

2.12. Statistical Analysis. All statistical analysis was performed using GraphPad Prism software.

3. RESULTS AND DISCUSSION

3.1. Synthesis and Formulation of Peptide Spider NPs. Peptide spiders were designed to display two trafficking peptides at the end of a polymer "leg" of an octo-valent polymer "body" (Figure 1A). Peptide spiders were synthesized by adding stoichiometric ratios of a cysteine-terminated membrane-active transportant (GWTLNSAGYLLGKINLKALAALAKKILC) or tumor-penetrating ligand, iRGD (CRGDKGPDC), to 20,000 molecular weight 8-arm PEG linked via reducible orthopyridyl disulfide or nonreducible maleimide chemistries (Figure 1A). The targeting peptide, iRGD, was identified by in vivo phage display[30] and has been grafted onto many NP delivery systems for tumor targeting via binding $\alpha_v\beta_3$ integrin.[44−46] We have used transportan in previous work to improve endosomal escape of internalized cargo.[15,47] After synthesis, substitution of the materials was confirmed by MALDI to be between 60 and 80% reaction efficiency (Supporting Information Figure S1). Concentrations of conjugate were calculated based on absorbance of tryptophans in the transportan peptide by UV−vis spectroscopy and therefore all concentrations used in subsequent formulations were standardized by the amount of transportan peptide. The resulting peptide spider conjugates were formulated into NPs by adding equal volumes of conjugates to siRNA and mixing rapidly, as has been previously described for other electrostatic complexes.[48] The formation of spherical particles was confirmed by TEM after negative staining with phosphotungstic acid (Figures 1A and S2). In order to confirm the diameters in aqueous solution as opposed to the dry conditions in TEM, we performed dynamic light scattering (DLS). Nonreducible or reducible peptide spider NPs (PSNPs) were formulated at ratios of conjugate/siRNA between 0.25 and 8, corresponding to N/P ratios between 0.156 and 5, as calculated from basic amino acids in transportan and phosphates in siRNA. The resulting hydrodynamic diameters were measured with DLS in water and in physiological levels of salt simulated by PBS up to 6 h after formulation, indicating that the NPs were stable (Figure 1B).

https://dx.doi.org/10.1021/acs.molpharmaceut.0c00714
Mol. Pharmaceutics 2020, 17, 3633−3642

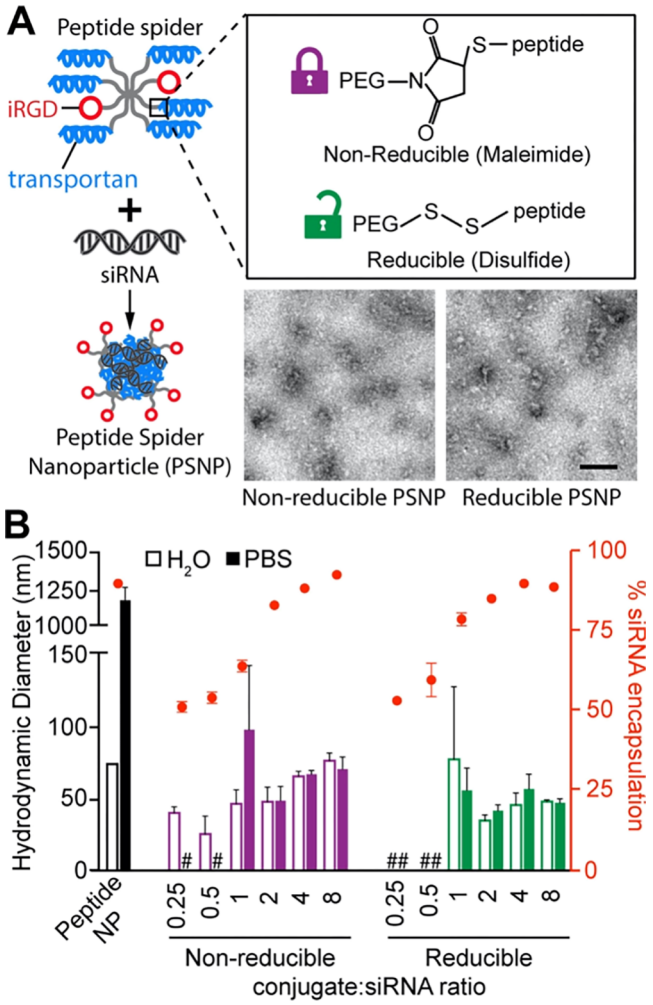

Figure 1. Design of PSNPs. (A) Schematic of a peptide spider. Eight-arm PEG is modified with trafficking peptides via nonreducible/reducible linkages and can condense siRNA. TEM of NPs formed with peptide spider conjugates reveal spherical NPs (scale bar = 100 nm). (B) Hydrodynamic diameters measured by DLS in water (empty bars) or PBS (solid bars). Diameters that could not be measured because of poor particle formation are denoted by a #. Percent siRNA encapsulation of corresponding NPs denoted by red circles (right *y*-axis; n = 3, mean + SD).

For PSNPs that formed NPs, zeta potential measurements were made and surface potentials were found to be near neutral (Supporting Information Figure S2). Encapulsation efficiency of siRNA was measured using a gel retardation assay, in which uncomplexed siRNA migrates into an agarose gel (Figure 1B). At conjugate to siRNA ratios above 2, when siRNA encapsulation was greater than 75%, both nonreducible and reducible peptide spider conjugates were able to form particles smaller than 100 nm in diameter. The measured hydrodynamic diameters of these particles were the same in water and in PBS, indicating that these particles were stable in physiological levels of salt. Peptide NPs with no PEG when formulated at a ratio that fully encapsulated siRNA had diameters less than 100 nm but aggregated in the presence of PBS to have diameters larger than 1 μm, as observed previously.[16] We used a Malvern NanoSight to measure NP concentrations prepared at a 4:1 peptide conjugate/siRNA ratio and both nonreducible and reducible PSNPs formulations were measured to be ~5 × 10^8 NPs/mL.

3.2. Silencing Activity of PSNPs. Having established the ability to form NPs with the peptide spider conjugates, a series of assays to evaluate function and trafficking within cells was completed. First, materials were evaluated in a reporter cell line stably expressing luciferase, OVCAR-8. Downregulation of luciferase enzyme as measured by luciferase activity normalized by the protein content (left axis) and cell viability (MTS assay, red diamonds; right axis) were measured 48 h after treatment with NPs formulated at peptide spider/siRNA ratios of 2, 4, and 8 and treated at a final siRNA concentration of 100 or 200 nM (Figure 2). 100% activity was determined by lysing untreated cells and measuring luciferase activity. All luminescence values were normalized by the protein content as measured by BCA assay to account for toxicity in addition to viability measurements with the MTS assay. As expected, free siRNA did not result in any silencing. The commercial reagent Lipofectamine RNAiMAX resulted in greater than 80% silencing, and was used to validate siRNA sequences in vitro. However, Lipofectamine cannot be evaluated in systemic in vivo delivery because of the well-document toxicity of cationic liposomes.[49] Both nonreducible and reducible PSNPs were able to mediate ~50% silencing while maintaining viability above 80%. Based on titration of NP concentration and formulation ratios, reducible PSNPs appeared to be more effective at silencing compared to nonreducible PSNPs. All subsequent studies were performed with peptide spider/siRNA ratios of 4.

3.3. Intracellular Distribution of PSNPs. Increased silencing activity, as observed for reducible PSNPs, may be attributable to several factors. One hypothesis is differential intracellular trafficking of cargo. To test this hypothesis, OVCAR-8 cells were imaged by microscopy after internalization of NPs prepared with fluorescently labeled siRNA. PSNPs were incubated at 37 °C with cells for 2 h, washed, and fixed in triplicate. Once NPs are internalized into cells, they are typically found in endosomes, and if they cannot escape into the cytosol, endosomes will mature into lysosomes.[50] Cells were labeled for lysosomes [lysosomal-associated membrane protein 1 (LAMP1)], filamental actin (phalloidin), and nuclei (Hoechst) and imaged by microscopy (Figure 3). As expected, no siRNA signal was detected in untreated cells. Comparison of siRNA distribution after delivery with nonreducible and reducible peptide spiders reveals that both materials are able to enter cells, but that reducible PSNPs lead to diffuse cytosolic siRNA with few puncta compared to the appearance of distinctly punctate siRNA signal in nonreducible PSNP-treated cells (Figure 3, insets). This observation suggests that linkage of peptides through reducible disulfide bonds leads to increased endosomal escape of cargo siRNA. It is also possible that the diffuse versus punctate appearance of siRNA is due to more stable complexation in NPs made with nonreducible compared to reducible polymers. Based on glutathione levels measured in endocytic vesicles,[51] peptides could separate from the PEG polymer backbone in peptide spiders made with reducible bonds, leading to the subsequent release of siRNA cargo and a more diffuse appearance.

3.4. Cell-Association of PSNPs in Cells with Low and High Receptor Expression. The discrepancy in the efficacy of silencing by nonreducible versus reducible PSNPs might also be due to differential association of material with cells. Increased association of NPs can yield increased silencing activity, as elevated concentrations of siRNA NPs can enhance silencing activity, as observed when cells are incubated with

https://dx.doi.org/10.1021/acs.molpharmaceut.0c00714
Mol. Pharmaceutics 2020, 17, 3633−3642

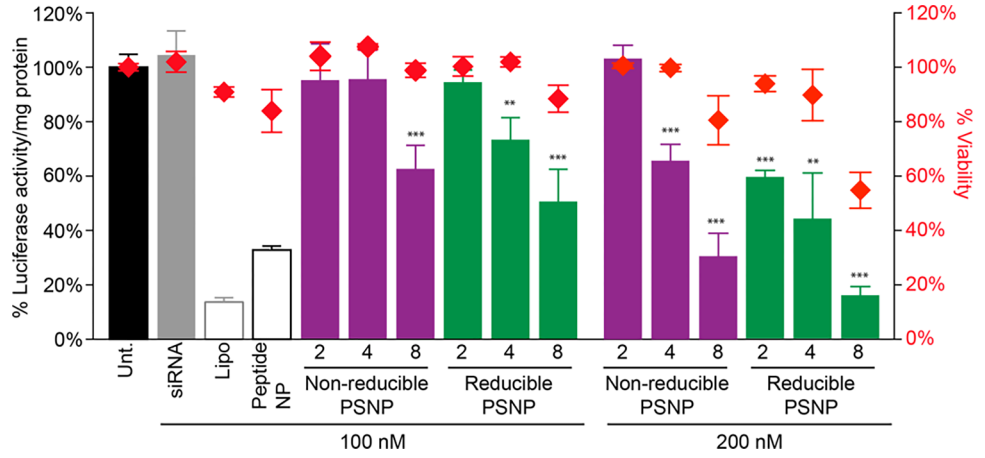

Figure 2. Silencing activity of peptide spiders. Nonreducible and reducible PSNPs carrying siRNA against luciferase formulated at 2, 4, and 8 conjugate/siRNA ratios were delivered to a reporter cell line stably expressing luciferase. Luciferase activity normalized by the protein content (left *y*-axis; bars) and cell viability assayed by MTS (right *y*-axis; red diamonds) were measured 48 h after treatment with NPs (n = 3, mean ± SD). Controls included untreated cells, free siRNA, commercial reagent Lipofectamine RNAiMAX, and peptide NPs. (**p < 0.01, ***p < 0.001 one-way ANOVA with Dunnett's post test).

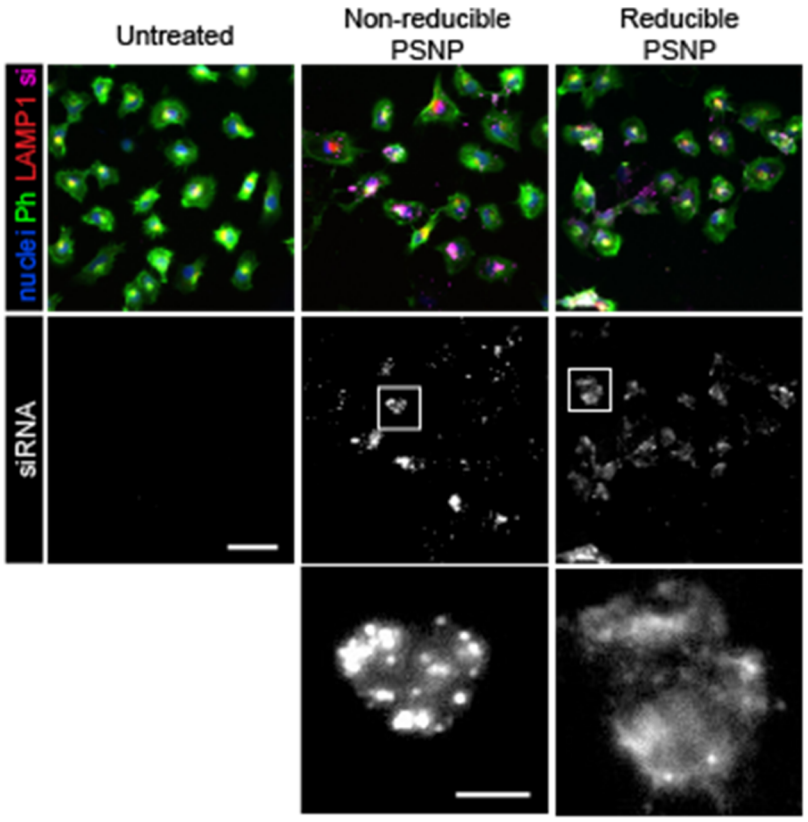

Figure 3. Intracellular distribution of PSNPs. Cells were incubated with nonreducible and reducible PSNPs carrying fluorescently labeled siRNA (Cy5; magenta) for 2 h and fixed and stained. Cells were imaged for nuclei (Hoechst; blue), microtubules (Phalloidin; green), and lysosomes (LAMP1; red) using microscopy (scale bar = 50 μm). Bottom row shows the enlargement of white box in siRNA image (scale bar = 10 μm; representative images from n = 3 study; study repeated in independent experiments).

PSNPs at a final siRNA concentration of 200 nM (Figure 2). To investigate the association of PSNPs with cells, two cell lines with low and high expression of the iRGD receptors were employed for binding studies. The cognate receptors for iRGD are integrin heterodimers, most prominently $\alpha_v\beta_3/\beta_5$ integrins.[30] Two human cancer cell lines were evaluated for their receptor expression by flow cytometry; U937, a human lymphoma cell line, expresses low levels of $\alpha_v\beta_3$ and α_v while MDA-MB-435S, a human melanoma cell line, expresses high levels of both (Figure 4A). Nonreducible and reducible PSNPs were formulated with fluorescently labeled siRNA at a peptide spider/siRNA ratio of 4 and incubated with cells at the indicated concentrations for 1 h at 4 °C. Cells were prechilled to 4 °C to inhibit internalization machinery within cells.[52] After removal of free NPs with washing, signal of fluorescently labeled siRNA was quantified with flow cytometry. Both

https://dx.doi.org/10.1021/acs.molpharmaceut.0c00714
Mol. Pharmaceutics 2020, 17, 3633−3642

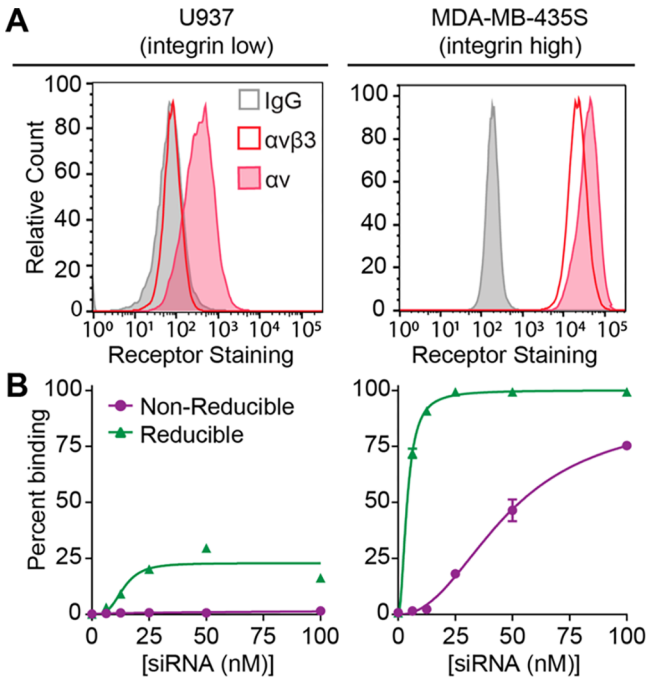

Figure 4. Cell association of PSNPs. (A) U937 and MDA-MB-435S cell lines were characterized for α_v and $\alpha_v\beta_3$ integrin staining using flow cytometry. (B) Association of nonreducible and reducible PSNPs carrying fluorescently labeled siRNA with U937 cells (left) or MDA-MB-435S cells (right) at several concentrations (n = 3, mean ± SD).

nonreducible and reducible PSNPs had increased signal in integrin-high MDA-MB-435 cells over integrin-low U937 cells (Figure 4B). Furthermore, based on this analysis, reducible PSNPs had increased fluorescence signal with cells compared with nonreducible PSNPs, which may have contributed, at least partly, to the increased silencing activity observed when cells were treated with reducible PSNPs (Figure 2). Although it was not expected that reducible PSNPs would have more associated fluorescence signal with cells compared to nonreducible PSNPs, it may be due to the differences in the sizes of the 8-arm PEG backbones, which were synthesized by two different vendors. Although both reducible and nonreducible backbones were purchased at 20 kDa sizes for comparison, when the materials were characterized by MALDI they were measured to be 14 kDa for PEG with reducible linkages and 20 kDa for PEG with nonreducible linkages. We do not believe the 30% difference in backbone size is responsible for the markedly different intracellular distributions (Figure 3) because they formed similarly sized NPs (Figure 1B). We also note that at 100 nM concentration of siRNA, total binding is similar between reducible and nonreducible PSNPs (Figure 4), and both the transfection and imaging study were conducted at this concentration of siRNA or higher (Figures 2 and 3).

3.5. Pharmacokinetics of PSNP Accumulation in the Tumor Model. Having established that peptide spiders were able to form NPs that exhibit silencing activity, we applied them to a mouse model of cancer. Using the MDA-MB-435S cell line that expresses a high level of integrin (Figure 3A), tumor cells were implanted subcutaneously into both flanks of nude mice. Once the resulting tumors reached 200−300 mm^3 in volume, studies were conducted. NPs were formulated at 4:1 ratio of peptide spider/siRNA at a 10 μM final siRNA concentration, 10-fold higher than what was used in vitro, in order to obtain volumes suitable for in vivo administration. Hydrodynamic diameters were measured at this concentration because it is known that formulation concentration affects particle sizes. Diameters of PSNP formulated at 10 μM were ∼100 nm, moderately bigger than those measured at 1 μM final siRNA concentration used for in vitro studies (Figure 1B) but diameters were still reasonable for systemic vascular delivery. By contrast, peptide without PEG formed particles with diameters >1 μm when formulated at high 10 μM concentrations compared to the ∼80 nm diameters when formulated at 1 μM concentrations (Figure 1B). Previous reports in the literature have shown that the diameters of NPs formed by electrostatic self assembly are concentration dependent.[53,54] Although it is unknown whether the large, micrometer-scaled particles formed using peptide without PEG are due to particle formation or rapid aggregation, the introduction of PEG improved the formulation of NPs with small hydrodynamic diameters suitable for intravenous application. In physiological levels of salt simulated by PBS, both nonreducible and reducible PSNPs maintained diameters ∼100 nm, similar sizes formed in water (Figure 5A). NPs were

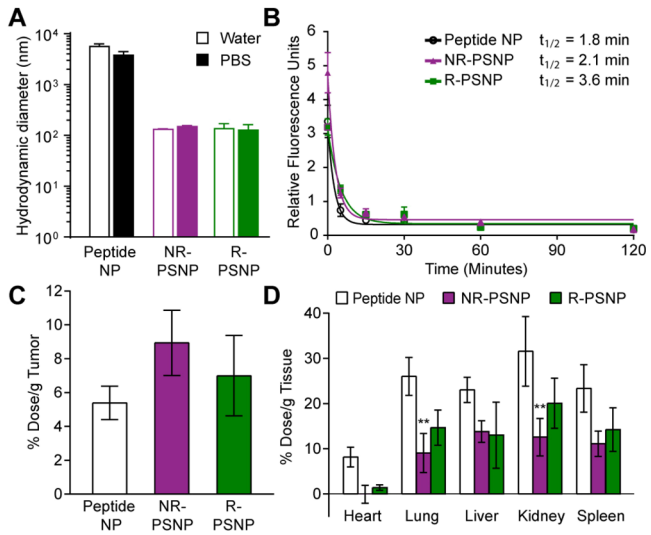

Figure 5. Pharmacokinetics of PSNPs. (A) Sizes of nonreducible and reducible PSNPs measured by DLS made at high concentrations (10 μM) suitable for in vivo injections. (B) Blood half-life of nonreducible and reducible PSNPs after intravenous delivery in mice (n = 3, mean ± SEM). Measurement of PSNPs carrying fluorescently labeled siRNA in (C) tumors and (D) organs 3 h after intravenous administration in mice bearing subcutaneous tumors (n = 3, mean ± SEM). (**p < 0.01 2-way ANOVA with Tukey's post test).

administered to mice at a 1 nmol dose via the tail vein, and blood half-life was measured by sampling 10 μL of blood for a period of 2 h (Figure 5B). Half-lives were on the order of minutes for all NPs; half-lives were 1.8 min for peptide NPs, 2.1 min for NR-PSNPs, and 3.6 min for R-PSNPs. Three hours after administration of NPs, mice were sacrificed and the tumors, heart, lung, liver, kidney, and spleen were dissected and processed to create tissue lysates. Fluorescence signal of VivoTag-S 750-labeled siRNA was measured in the supernatant (Figure 5C,D). A slight increase in material was detected in tumors from mice that received PSNPs compared to peptide NPs, although it was not statistically significant (Figure 5C). The observation that active targeting may not significantly affect bulk biodistribution, but is critical for cell-

https://dx.doi.org/10.1021/acs.molpharmaceut.0c00714
Mol. Pharmaceutics 2020, 17, 3633−3642

specific interaction and/or retention in the tissue, has been observed consistently in the literature.[55−57] Consistent with what has been observed with large particle accumulation in organs of the reticuloendothelial system,[58] PSNPs had less accumulation in off-target organs compared to NPs made with no PEG (Figure 5D). In particular, nonreducible PSNPs had significantly less accumulation in the lung and kidney, relative to peptide NPs. However, it is noted that there is significant off-target organ accumulation of the PSNPs.[59] Similarly, PEG lipid NPs that are the basis for the only FDA-approved siRNA drug Onpattro are observed to accumulate in the liver and spleen[4,60] and reducing off-target organ accumulation for tumor delivery remains an outstanding challenge for the field.

3.6. Tissue Distribution of PSNPs in Tumors. The accumulation of materials within the tumor tissue were investigated by administering PSNPs made with 1 nmol of FAM-labeled siRNA at 24, 3, and 1 h before harvesting of tumors (Figure 6). Tumors were sectioned and the FAM label

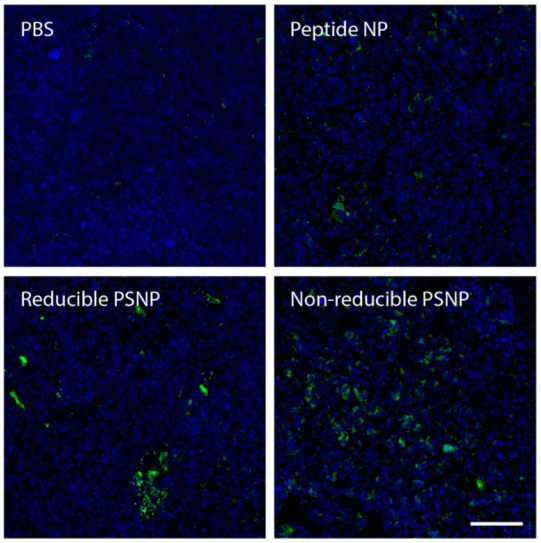

Figure 6. Tissue distribution of PSNP in the tumor tissue. Mice were dosed with 1 nmol of FAM-labeled siRNA dosed at 24, 3, and 1 h before tumors were excised. Tumors were sectioned and the siRNA signal was amplified using immunolabeling (green) and sections counterstained for nuclei (Hoechst; blue). Representative areas of the tumor are shown (n = 3−4 tumors per condition, scale bar = 100 μm).

amplified using immunolabeling. Relative levels of siRNA detected in the tumor by nonreducible PSNPs was higher than peptide NPs and reducible PSNPs. Furthermore, reducible PSNP-delivered siRNA appeared to be restricted in tissue areas compared to a more distributed appearance of nonreducible PSNP-delivered siRNA. This relative difference may be attributed to reduction of the linkage and subsequent dissociation of trafficking peptides from the PEG backbone in the biological environment of the blood or tumor tissue.

3.7. Activity of PSNPs in Tumor Models. Last, we looked at the ability of our PSNP system to downregulate target proteins. To do this, we formulated NPs with siRNA against the transcription factor ID4, known to be upregulated in tumors,[14] and administered 2 nmol of siRNA per dose (or 1.4 mg/kg) at 6, 4, and 2 days before harvesting tissue. Past reports on systemically delivered peptide-based delivery systems for siRNA in the literature have been administered at siRNA doses between 0.5 and 1.7 mg/kg.[61−64] We first looked at toxicity of these materials under the conditions of repeat dosing. The heart, lung, liver, kidney, and spleen were embedded in paraffin and stained with hematoxylin and eosin. A pathologist blinded to the conditions of the mice inspected the tissue and found no signs of toxicity in any tissue. Representative images of triplicate samples are shown in Figure 7. The knockdown of the target protein ID4 was analyzed in

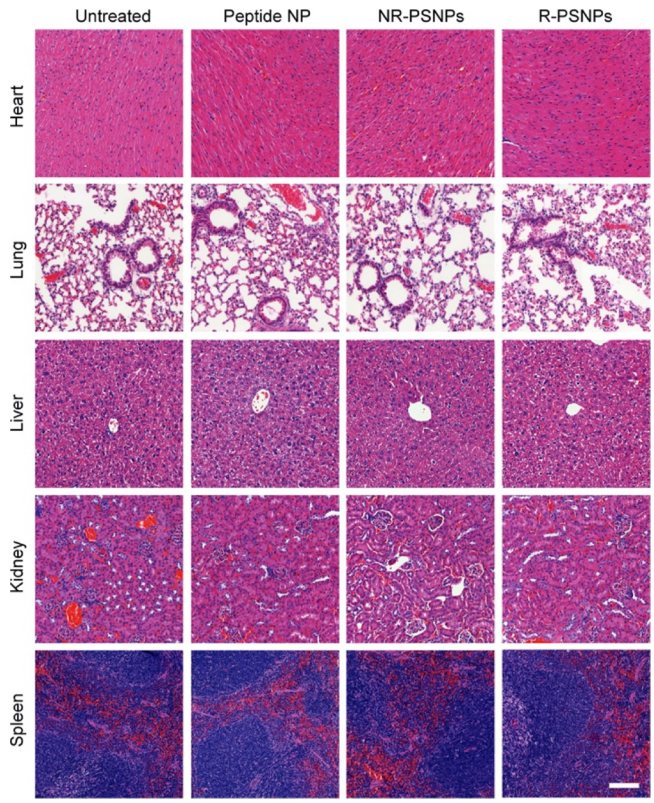

Figure 7. Toxicity of PSNPs. Hematoxylin and eosin staining of the heart, lung, liver, kidney, and spleen from mice administered 3 doses of NPs (scale bar = 100 μm; n = 3, representative images shown).

tumor lysates using Western blotting (Figure 8A). Nonreducible PSNPs were able to mediate ∼60% downregulation of ID4 protein, whereas reducible PSNPs mediated ∼30% downregulation and nonPEGylated peptide NPs did not mediate significant downregulation in this dosing scheme. These results were unexpected because reducible PSNPs outperformed nonreducible PSNPs when evaluated in vitro. However, there are multiple trafficking barriers that occur before NPs reach their target cells (e.g., blood protein interactions, off-target organ accumulation, and tissue extravasation), which cannot be predicted by culture model systems. We hypothesized that reduction of the linkage keeping peptides on the PEG backbone could cause destabilization of reducible PSNPs before they could reach their target destination either in the blood or the tumor microenvironment. To test this prediction, we incubated nonreducible and reducible PSNPs with the reducing agent dithiothreitol (DTT) at 5 mM in PBS and monitored their hydrodynamic diameters over time (Figure 8B). Whereas nonreducible PSNPs were unaffected by treatment with DTT as expected, reducible PSNPs had increasing diameters over time, indicating removal of the PEG shielding and particle aggregation (Figure 8C).

https://dx.doi.org/10.1021/acs.molpharmaceut.0c00714
Mol. Pharmaceutics 2020, 17, 3633−3642

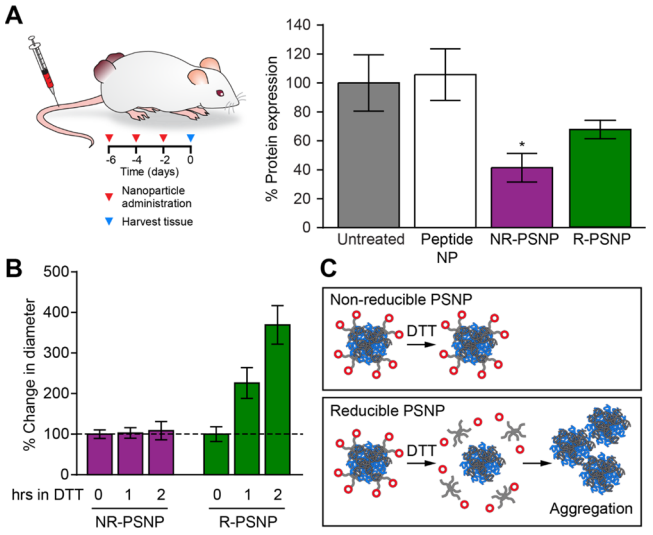

Figure 8. Silencing efficacy of PSNPs in vivo. (A) Time line of NP administration. Right, ID4 protein knockdown in the flank model of MDA-MB-435S tumors after treatment with nonreducible or reducible PSNPs (n = 4, mean ± SEM, *p < 0.05 one-way ANOVA with Dunnett's post test). (B) Changes in hydrodynamic diameters of PSNPs from time 0 after treatment with the reducing agent, DTT at 5 mM (n = 3, mean ± SD). (C) Schematic of the proposed mechanism of DTT initiated aggregation.

The NP aggregation of reducible PSNPs may have contributed to the decreased silencing activity observed (Figure 8A). The aggregation of reducible PSNPs prior to reaching tumors cells is also supported by the appearance of concentrated siRNA signal in tumors compared to the diffuse siRNA signal in tumors after nonreducible PSNP delivery (Figure 6). Our observations are in contrast to other reducible siRNA delivery systems in the literature that achieve robust silencing.[65−67] In our system, transportan peptide is required for both intracellular release and siRNA binding through the multiple cationic amino acid residues. Therefore, reduction of the disulfide bond separates the siRNA binding component from PEG, which is required for stability of the NPs. In previous examples of reducible systems, disulfide bonds were used to stabilize siRNA to siRNA interactions[66] or attach endosomal escape components with siRNA binding/stabilizing components.[65] Other factors that may contribute to differences in stability of various disulfide cross-linked NPs that still require further investigation are the relative stability of the NPs themselves, the number of disulfide cross-links, the local chemical environment of the disulfide bonds, and the steric shielding of the disulfide bonds.[68]

4. CONCLUSIONS

In this work, we engineered a material to deliver nucleic acids using a polymeric backbone grafted with trafficking peptides. We investigated the stability of the linker used to attach peptides to the polymeric backbone and found that although a reducible linker can lead to more efficient delivery in cultured cells, a nonreducible linker was more effective at functional delivery to tumors in animal models. This finding highlights the need for holistic consideration of trafficking barriers in the design of systemically delivered nucleic acid carriers, where optimal design criteria between intracellular and systemic delivery may be conflicting. In one well-documented example of the need to balance design criteria of gene carriers intended for systemic delivery, PEG is added to FDA-approved NP formulations in order to improve pharmacokinetics,[69] even though it is known that PEG reduces gene silencing activity.[43] Alternatively, the advantage of reducible bonds to confer silencing activity could be capitalized through local delivery, such as intratumoral injection; intratumoral injection is a particularly promising route of administration for immunotherapy.[70,71] In summary, this work offers an insight into the stability of peptide−polymer hybrid materials for use in nucleic acid delivery.

■ ASSOCIATED CONTENT

Supporting Information

The Supporting Information is available free of charge at https://pubs.acs.org/doi/10.1021/acs.molpharmaceut.0c00714.

MALDI of peptide conjugates, TEM of NPs, and zeta potential measurements of NPs (PDF)

■ AUTHOR INFORMATION

Corresponding Authors

Ester J. Kwon − *Koch Institute for Integrative Cancer Research, Massachusetts Institute of Technology, Cambridge, Massachusetts 02139, United States;* orcid.org/0000-0002-6335-9681; Email: ejkwon@ucsd.edu

Sangeeta N. Bhatia − *Institute for Medical Engineering and Science, Department of Electrical and Computer Science, and Marble Center for Cancer Nanomedicine, Massachusetts Institute of Technology, Cambridge, Massachusetts 02139, United States; Department of Medicine, Brigham and Women's Hospital, Boston, Massachusetts 02115, United States; Broad Institute of Massachusetts of Technology and Harvard, Cambridge, Massachusetts 02139, United States; Howard Hughes Medical Institute, Chevy Chase, Maryland 20815, United States*; Email: sbhatia@mit.edu

Author

Henry Ko − *Koch Institute for Integrative Cancer Research, Massachusetts Institute of Technology, Cambridge, Massachusetts 02139, United States*

Complete contact information is available at: https://pubs.acs.org/10.1021/acs.molpharmaceut.0c00714

Author Contributions

○E.J.K. and H.K contributed equally.

Notes

The authors declare no competing financial interest.

The authors declare that all data supporting the findings of this study are available in the paper.

■ ACKNOWLEDGMENTS

The authors thank Dr. Heather Fleming (MIT) for critical reading of the article. We thank the Koch Institute Swanson Biotechnology Core at MIT. This study was supported in part by a Koch Institute Support Grant P30-CA14051 from the National Cancer Institute (Swanson Biotechnology Center), a Core Center Grant P30-ES002109 from the National Institute of Environmental Health Sciences, the Ludwig Fund for Cancer Research, and the Koch Institute Marble Center for Cancer Nanomedicine. E.J.K. acknowledges funding from the NIH (F32CA177094). S.N.B. is a Howard Hughes Medical Institute Investigator.

https://dx.doi.org/10.1021/acs.molpharmaceut.0c00714
Mol. Pharmaceutics 2020, 17, 3633−3642

REFERENCES

(1) Yin, H.; Kanasty, R. L.; Eltoukhy, A. A.; Vegas, A. J.; Dorkin, J. R.; Anderson, D. G. Non-Viral Vectors for Gene-Based Therapy. *Nat. Rev. Genet.* **2014**, *15*, 541−555.

(2) Richner, J. M.; Himansu, S.; Dowd, K. A.; Butler, S. L.; Salazar, V.; Fox, J. M.; Julander, J. G.; Tang, W. W.; Shresta, S.; Pierson, T. C.; Ciaramella, G.; Diamond, M. S. Modified MRNA Vaccines Protect against Zika Virus Infection. *Cell* **2017**, *168*, 1114−1125.e10.

(3) Davis, M. E.; Zuckerman, J. E.; Choi, C. H. J.; Seligson, D.; Tolcher, A.; Alabi, C. A.; Yen, Y.; Heidel, J. D.; Ribas, A. Evidence of RNAi in Humans from Systemically Administered SiRNA via Targeted Nanoparticles. *Nature* **2010**, *464*, 1067−1070.

(4) Akinc, A.; Maier, M. A.; Manoharan, M.; Fitzgerald, K.; Jayaraman, M.; Barros, S.; Ansell, S.; Du, X.; Hope, M. J.; Madden, T. D.; Mui, B. L.; Semple, S. C.; Tam, Y. K.; Ciufolini, M.; Witzigmann, D.; Kulkarni, J. A.; van der Meel, R.; Cullis, P. R. The Onpattro Story and the Clinical Translation of Nanomedicines Containing Nucleic Acid-Based Drugs. *Nat. Nanotechnol.* **2019**, *14*, 1084−1087.

(5) Fosgerau, K.; Hoffmann, T. Peptide Therapeutics: Current Status and Future Directions. *Drug Discovery Today* **2015**, *20*, 122−128.

(6) Walensky, L. D.; Bird, G. H. Hydrocarbon-Stapled Peptides: Principles, Practice, and Progress. *J. Med. Chem.* **2014**, *57*, 6275−6288.

(7) Sheridan, C. Proof of concept for next-generation nanoparticle drugs in humans. *Nat. Biotechnol.* **2012**, *30*, 471.

(8) Endoh, T.; Ohtsuki, T. Cellular SiRNA Delivery Using Cell-Penetrating Peptides Modified for Endosomal Escape. *Adv. Drug Delivery Rev.* **2009**, *61*, 704−709.

(9) Eguchi, A.; Meade, B. R.; Chang, Y.-C.; Fredrickson, C. T.; Willert, K.; Puri, N.; Dowdy, S. F. Efficient SiRNA Delivery into Primary Cells by a Peptide Transduction Domain−DsRNA Binding Domain Fusion Protein. *Nat. Biotechnol.* **2009**, *27*, 567−571.

(10) Whitehead, K. A.; Langer, R.; Anderson, D. G. Knocking down Barriers: Advances in SiRNA Delivery. *Nat. Rev. Drug Discovery* **2009**, *8*, 129−138.

(11) Ruoslahti, E.; Bhatia, S. N.; Sailor, M. J. Targeting of Drugs and Nanoparticles to Tumors. *J. Cell Biol.* **2010**, *188*, 759−768.

(12) McCarthy, J.; Weissleder, R. Multifunctional Magnetic Nanoparticles for Targeted Imaging and Therapy. *Adv. Drug Delivery Rev.* **2008**, *60*, 1241−1251.

(13) Byrne, J. D.; Betancourt, T.; Brannon-Peppas, L. Active Targeting Schemes for Nanoparticle Systems in Cancer Therapeutics. *Adv. Drug Delivery Rev.* **2008**, *60*, 1615−1626.

(14) Ren, Y.; Cheung, H. W.; von Maltzhan, G.; Agrawal, A.; Cowley, G. S.; Weir, B. A.; Boehm, J. S.; Tamayo, P.; Karst, A. M.; Liu, J. F.; Hirsch, M. S.; Mesirov, J. P.; Drapkin, R.; Root, D. E.; Lo, J.; Fogal, V.; Ruoslahti, E.; Hahn, W. C.; Bhatia, S. N. Targeted Tumor-Penetrating SiRNA Nanocomplexes for Credentialing the Ovarian Cancer Oncogene ID4. *Sci. Transl. Med.* **2012**, *4*, 147ra112.

(15) Ren, Y.; Hauert, S.; Lo, J. H.; Bhatia, S. N. Identification and Characterization of Receptor-Specific Peptides for SiRNA Delivery. *ACS Nano* **2012**, *6*, 8620−8631.

(16) Lo, J. H.; Kwon, E. J.; Zhang, A. Q.; Singhal, P.; Bhatia, S. N. Comparison of Modular PEG Incorporation Strategies for Stabilization of Peptide−SiRNA Nanocomplexes. *Bioconjugate Chem.* **2016**, *27*, 2323−2331.

(17) Bolhassani, A. Potential Efficacy of Cell-Penetrating Peptides for Nucleic Acid and Drug Delivery in Cancer. *Biochim. Biophys. Acta* **2011**, *1816*, 232−246.

(18) Nakase, I.; Akita, H.; Kogure, K.; Gräslund, A.; Langel, Ü.; Harashima, H.; Futaki, S. Efficient Intracellular Delivery of Nucleic Acid Pharmaceuticals Using Cell-Penetrating Peptides. *Acc. Chem. Res.* **2012**, *45*, 1132−1139.

(19) Lehto, T.; Ezzat, K.; Wood, M. J. A.; EL Andaloussi, S. Peptides for Nucleic Acid Delivery. *Adv. Drug Delivery Rev.* **2016**, *106*, 172−182.

(20) Lächelt, U.; Wagner, E. Nucleic Acid Therapeutics Using Polyplexes: A Journey of 50 Years (and Beyond). *Chem. Rev.* **2015**, *115*, 11043−11078.

(21) Tan, J.-K. Y.; Sellers, D. L.; Pham, B.; Pun, S. H.; Horner, P. J. Non-Viral Nucleic Acid Delivery Strategies to the Central Nervous System. *Front. Mol. Neurosci.* **2016**, *9*, 108.

(22) van Vlerken, L. E.; Vyas, T. K.; Amiji, M. M. Poly(Ethylene Glycol)-Modified Nanocarriers for Tumor-Targeted and Intracellular Delivery. *Pharm. Res.* **2007**, *24*, 1405−1414.

(23) Mishra, S.; Webster, P.; Davis, M. E. PEGylation Significantly Affects Cellular Uptake and Intracellular Trafficking of Non-Viral Gene Delivery Particles. *Eur. J. Cell Biol.* **2004**, *83*, 97−111.

(24) Hatakeyama, H.; Akita, H.; Harashima, H. The Polyethyleneglycol Dilemma: Advantage and Disadvantage of PEGylation of Liposomes for Systemic Genes and Nucleic Acids Delivery to Tumors. *Biol. Pharm. Bull.* **2013**, *36*, 892−899.

(25) Jackson, M. A.; Bedingfield, S. K.; Yu, F.; Stokan, M. E.; Miles, R. E.; Curvino, E. J.; Hoogenboezem, E. N.; Bonami, R. H.; Patel, S. S.; Kendall, P. L.; Giorgio, T. D.; Duvall, C. L. Dual Carrier-Cargo Hydrophobization and Charge Ratio Optimization Improve the Systemic Circulation and Safety of Zwitterionic Nano-Polyplexes. *Biomaterials* **2019**, *192*, 245−259.

(26) Suk, J. S.; Xu, Q.; Kim, N.; Hanes, J.; Ensign, L. M. PEGylation as a Strategy for Improving Nanoparticle-Based Drug and Gene Delivery. *Adv. Drug Delivery Rev.* **2016**, *99*, 28−51.

(27) Werfel, T. A.; Jackson, M. A.; Kavanaugh, T. E.; Kirkbride, K. C.; Miteva, M.; Giorgio, T. D.; Duvall, C. Combinatorial Optimization of PEG Architecture and Hydrophobic Content Improves Ternary SiRNA Polyplex Stability, Pharmacokinetics, and Potency in Vivo. *J. Controlled Release* **2017**, *255*, 12−26.

(28) Deshayes, S.; Morris, M.; Heitz, F.; Divita, G. Delivery of Proteins and Nucleic Acids Using a Non-Covalent Peptide-Based Strategy. *Adv. Drug Delivery Rev.* **2008**, *60*, 537−547.

(29) He, D.; Wagner, E. Defined Polymeric Materials for Gene Delivery. *Macromol. Biosci.* **2015**, *15*, 600−612.

(30) Sugahara, K. N.; Teesalu, T.; Karmali, P. P.; Kotamraju, V. R.; Agemy, L.; Girard, O. M.; Hanahan, D.; Mattrey, R. F.; Ruoslahti, E. Tissue-Penetrating Delivery of Compounds and Nanoparticles into Tumors. *Cancer Cell* **2009**, *16*, 510−520.

(31) Sugahara, K. N.; Teesalu, T.; Karmali, P. P.; Kotamraju, V. R.; Agemy, L.; Greenwald, D. R.; Ruoslahti, E. Coadministration of a Tumor-Penetrating Peptide Enhances the Efficacy of Cancer Drugs. *Science* **2010**, *328*, 1031−1035.

(32) Gu, G.; Gao, X.; Hu, Q.; Kang, T.; Liu, Z.; Jiang, M.; Miao, D.; Song, Q.; Yao, L.; Tu, Y.; Pang, Z.; Chen, H.; Jiang, X.; Chen, J. The Influence of the Penetrating Peptide IRGD on the Effect of Paclitaxel-Loaded MT1-AF7p-Conjugated Nanoparticles on Glioma Cells. *Biomaterials* **2013**, *34*, 5138−5148.

(33) Yan, F.; Wu, H.; Liu, H.; Deng, Z.; Liu, H.; Duan, W.; Liu, X.; Zheng, H. Molecular Imaging-Guided Photothermal/Photodynamic Therapy against Tumor by IRGD-Modified Indocyanine Green Nanoparticles. *J. Controlled Release* **2016**, *224*, 217−228.

(34) Weissleder, R.; Kelly, K.; Sun, E. Y.; Shtatland, T.; Josephson, L. Cell-Specific Targeting of Nanoparticles by Multivalent Attachment of Small Molecules. *Nat. Biotechnol.* **2005**, *23*, 1418−1423.

(35) Hammarström, S. Binding of Helix Pomatia A Hemagglutinin to Human Erythrocytes and Their Cells. Influence of Multivalent Interaction on Affinity. *Scand. J. Immunol.* **1973**, *2*, 53−66.

(36) Collins, B. E.; Paulson, J. C. Cell Surface Biology Mediated by Low Affinity Multivalent Protein-Glycan Interactions. *Curr. Opin. Chem. Biol.* **2004**, *8*, 617−625.

(37) Skehel, J. J.; Wiley, D. C. Receptor Binding and Membrane Fusion in Virus Entry: The Influenza Hemagglutinin. *Annu. Rev. Biochem.* **2000**, *69*, 531−569.

(38) Lindwasser, O. W.; Resh, M. D. Multimerization of Human Immunodeficiency Virus Type 1 Gag Promotes Its Localization to Barges, Raft-Like Membrane Microdomains. *J. Virol.* **2001**, *75*, 7913−7924.

https://dx.doi.org/10.1021/acs.molpharmaceut.0c00714
Mol. Pharmaceutics 2020, 17, 3633−3642

(39) Maldarelli, F.; Chen, M. Y.; Willey, R. L.; Strebel, K. Human Immunodeficiency Virus Type 1 Vpu Protein Is an Oligomeric Type I Integral Membrane Protein. *J. Virol.* **1993**, *67*, 5056−5061.
(40) Kim, H.; Kitamatsu, M.; Ohtsuki, T. Enhanced Intracellular Peptide Delivery by Multivalent Cell-Penetrating Peptide with Bioreducible Linkage. *Bioorg. Med. Chem. Lett.* **2018**, *28*, 378−381.
(41) Zeng, H.; Little, H. C.; Tiambeng, T. N.; Williams, G. A.; Guan, Z. Multifunctional Dendronized Peptide Polymer Platform for Safe and Effective SiRNA Delivery. *J. Am. Chem. Soc.* **2013**, *135*, 4962−4965.
(42) Imani, R.; Prakash, S.; Vali, H.; Faghihi, S. Polyethylene Glycol and Octa-Arginine Dual-Functionalized Nanographene Oxide: An Optimization for Efficient Nucleic Acid Delivery. *Biomater. Sci.* **2018**, *6*, 1636−1650.
(43) Kanasty, R.; Dorkin, J. R.; Vegas, A.; Anderson, D. Delivery Materials for SiRNA Therapeutics. *Nat. Mater.* **2013**, *12*, 967−977.
(44) Chow, E. K.-H.; Ho, D. Cancer Nanomedicine: From Drug Delivery to Imaging. *Sci. Transl. Med.* **2013**, *5*, 216rv4.
(45) Peng, Z.-H.; Kopeček, J. Enhancing Accumulation and Penetration of HPMA Copolymer−Doxorubicin Conjugates in 2D and 3D Prostate Cancer Cells via IRGD Conjugation with an MMP-2 Cleavable Spacer. *J. Am. Chem. Soc.* **2015**, *137*, 6726−6729.
(46) Zhou, J.; Patel, T. R.; Fu, M.; Bertram, J. P.; Saltzman, W. M. Octa-Functional PLGA Nanoparticles for Targeted and Efficient SiRNA Delivery to Tumors. *Biomaterials* **2012**, *33*, 583−591.
(47) Kwon, E. J.; Skalak, M.; Lo Bu, R.; Bhatia, S. N. Neuron-Targeted Nanoparticle for SiRNA Delivery to Traumatic Brain Injuries. *ACS Nano* **2016**, *10*, 7926−7933.
(48) Pun, S. H.; Bellocq, N. C.; Liu, A.; Jensen, G.; Machemer, T.; Quijano, E.; Schluep, T.; Wen, S.; Engler, H.; Heidel, J.; Davis, M. E. Cyclodextrin-Modified Polyethylenimine Polymers for Gene Delivery. *Bioconjugate Chem.* **2004**, *15*, 831−840.
(49) Lv, H.; Zhang, S.; Wang, B.; Cui, S.; Yan, J. Toxicity of Cationic Lipids and Cationic Polymers in Gene Delivery. *J. Controlled Release* **2006**, *114*, 100−109.
(50) Sahay, G.; Querbes, W.; Alabi, C.; Eltoukhy, A.; Sarkar, S.; Zurenko, C.; Karagiannis, E.; Love, K.; Chen, D.; Zoncu, R.; Buganim, Y.; Schroeder, A.; Langer, R.; Anderson, D. G. Efficiency of SiRNA Delivery by Lipid Nanoparticles Is Limited by Endocytic Recycling. *Nat. Biotechnol.* **2013**, *31*, 653−658.
(51) Jiang, X.; Yu, Y.; Chen, J.; Zhao, M.; Chen, H.; Song, X.; Matzuk, A. J.; Carroll, S. L.; Tan, X.; Sizovs, A.; Cheng, N.; Wang, M. C.; Wang, J. Quantitative Imaging of Glutathione in Live Cells Using a Reversible Reaction-Based Ratiometric Fluorescent Probe. *ACS Chem. Biol.* **2015**, *10*, 864−874.
(52) Beisiegel, U.; Schneider, W. J.; Goldstein, J. L.; Anderson, R. G.; Brown, M. S. Monoclonal Antibodies to the Low Density Lipoprotein Receptor as Probes for Study of Receptor-Mediated Endocytosis and the Genetics of Familial Hypercholesterolemia. *J. Biol. Chem.* **1981**, *256*, 11923−11931.
(53) Grzelczak, M.; Vermant, J.; Furst, E. M.; Liz-Marzán, L. M. Directed Self-Assembly of Nanoparticles. *ACS Nano* **2010**, *4*, 3591−3605.
(54) Romøren, K.; Pedersen, S.; Smistad, G.; Evensen, Ø.; Thu, B. J. The Influence of Formulation Variables on in Vitro Transfection Efficiency and Physicochemical Properties of Chitosan-Based Polyplexes. *Int. J. Pharm.* **2003**, *261*, 115−127.
(55) Choi, C. H. J.; Alabi, C. A.; Webster, P.; Davis, M. E. Mechanism of Active Targeting in Solid Tumors with Transferrin-Containing Gold Nanoparticles. *Proc. Natl. Acad. Sci. U.S.A.* **2010**, *107*, 1235−1240.
(56) Bartlett, D. W.; Su, H.; Hildebrandt, I. J.; Weber, W. A.; Davis, M. E. Impact of Tumor-Specific Targeting on the Biodistribution and Efficacy of SiRNA Nanoparticles Measured by Multimodality in Vivo Imaging. *Proc. Natl. Acad. Sci.* **2007**, *104*, 15549−15554.
(57) Wang, J.; Lee, G. Y.; Lu, Q.; Peng, X.; Wu, J.; Wu, S.; Kairdolf, B. A.; Nie, S.; Wang, Y.; Lane, L. A. Quantitative Examination of the Active Targeting Effect: The Key Factor for Maximal Tumor Accumulation and Retention of Short-Circulated Biopolymeric Nanocarriers. *Bioconjugate Chem.* **2017**, *28*, 1351−1355.
(58) Jiang, W.; Kim, B. Y. S.; Rutka, J. T.; Chan, W. C. W. Nanoparticle-Mediated Cellular Response Is Size-Dependent. *Nat. Nanotechnol.* **2008**, *3*, 145−150.
(59) Wilhelm, S.; Tavares, A. J.; Dai, Q.; Ohta, S.; Audet, J.; Dvorak, H. F.; Chan, W. C. W. Analysis of Nanoparticle Delivery to Tumours. *Nat. Rev. Mater.* **2016**, *1*, 16014.
(60) Mui, B. L.; Tam, Y. K.; Jayaraman, M.; Ansell, S. M.; Du, X.; Tam, Y. Y. C.; Lin, P. J.; Chen, S.; Narayanannair, J. K.; Rajeev, K. G.; Manoharan, M.; Akinc, A.; Maier, M. A.; Cullis, P.; Madden, T. D.; Hope, M. J. Influence of Polyethylene Glycol Lipid Desorption Rates on Pharmacokinetics and Pharmacodynamics of SiRNA Lipid Nanoparticles. *Mol. Ther.–Nucleic Acids* **2013**, *2*, e139.
(61) Boisguérin, P.; Deshayes, S.; Gait, M. J.; O'Donovan, L.; Godfrey, C.; Betts, C. A.; Wood, M. J. A.; Lebleu, B. Delivery of Therapeutic Oligonucleotides with Cell Penetrating Peptides. *Adv. Drug Delivery Rev.* **2015**, *87*, 52−67.
(62) Crombez, L.; Morris, M. C.; Dufort, S.; Aldrian-Herrada, G.; Nguyen, Q.; Mc Master, G.; Coll, J.-L.; Heitz, F.; Divita, G. Targeting Cyclin B1 through Peptide-Based Delivery of SiRNA Prevents Tumour Growth. *Nucleic Acids Res.* **2009**, *37*, 4559−4569.
(63) Michiue, H.; Eguchi, A.; Scadeng, M.; Dowdy, S. F. Induction of in Vivo Synthetic Lethal RNAi Responses to Treat Glioblastoma. *Cancer Biol. Ther.* **2009**, *8*, 2304−2311.
(64) Hou, K. K.; Pan, H.; Ratner, L.; Schlesinger, P. H.; Wickline, S. A. Mechanisms of Nanoparticle-Mediated SiRNA Transfection by Melittin-Derived Peptides. *ACS Nano* **2013**, *7*, 8605−8615.
(65) Li, J.; Cheng, D.; Yin, T.; Chen, W.; Lin, Y.; Chen, J.; Li, R.; Shuai, X. Copolymer of Poly(Ethylene Glycol) and Poly(L-Lysine) Grafting Polyethylenimine through a Reducible Disulfide Linkage for SiRNA Delivery. *Nanoscale* **2014**, *6*, 1732−1740.
(66) Lee, S. J.; Yook, S.; Yhee, J. Y.; Yoon, H. Y.; Kim, M.-G.; Ku, S. H.; Kim, S. H.; Park, J. H.; Jeong, J. H.; Kwon, I. C.; Lee, S.; Lee, H.; Kim, K. Co-Delivery of VEGF and Bcl-2 Dual-Targeted SiRNA Polymer Using a Single Nanoparticle for Synergistic Anti-Cancer Effects in Vivo. *J. Controlled Release* **2015**, *220*, 631−641.
(67) Zhou, Z.; Li, H.; Wang, K.; Guo, Q.; Li, C.; Jiang, H.; Hu, Y.; Oupicky, D.; Sun, M. Bioreducible Cross-Linked Hyaluronic Acid/Calcium Phosphate Hybrid Nanoparticles for Specific Delivery of SiRNA in Melanoma Tumor Therapy. *ACS Appl. Mater. Interfaces* **2017**, *9*, 14576−14589.
(68) Oupický, D.; Li, J. Bioreducible Polycations in Nucleic Acid Delivery: Past, Present, and Future Trends. *Macromol. Biosci.* **2014**, *14*, 908−922.
(69) Garber, K. Alnylam launches era of RNAi drugs. *Nat. Biotechnol.* **2018**, *36*, 777.
(70) Aznar, M. A.; Tinari, N.; Rullán, A. J.; Sánchez-Paulete, A. R.; Rodriguez-Ruiz, M. E.; Melero, I. Intratumoral Delivery of Immunotherapy—Act Locally, Think Globally. *J. Immunol.* **2017**, *198*, 31−39.
(71) Wang, S.; Campos, J.; Gallotta, M.; Gong, M.; Crain, C.; Naik, E.; Coffman, R. L.; Guiducci, C. Intratumoral Injection of a CpG Oligonucleotide Reverts Resistance to PD-1 Blockade by Expanding Multifunctional CD8+ T Cells. *Proc. Natl. Acad. Sci.* **2016**, *113*, E7240−E7249.

https://dx.doi.org/10.1021/acs.molpharmaceut.0c00714
Mol. Pharmaceutics 2020, 17, 3633−3642